Evaluation of geometrically nonlinear effects due to large cross-sectional deformations of compact and shell-like structures

Evaluation of geometrically nonlinear effects due to large cross-sectional deformations of compact and shell-like structures

E. Carrera*, A. Pagani†, R. Augello‡

Mul^2 Group
Department of Mechanical and Aerospace Engineering, Politecnico di Torino
Corso Duca degli Abruzzi 24, 10129 Torino, Italy.

Abstract: *This paper investigates geometrically nonlinear effects due to large deformations over the cross-sections of beam-like and shell-like structures. Finite elements are used to provide numerical solutions along with the Newton-Raphson technique and the arc-length method. Refined theories able to capture cross-sectional deformation are constructed by referring to the Carrera Unified Formulation. Full nonlinear Green-Lagrange strains and second Piola-Kirchoff stresses are employed in a total Lagrangian scenario. The numerical results demonstrate that geometrical nonlinearities play a fundamental role when cross-sectional deformations become significant and theories of structures with nonlinear kinematics are utilized. In other words, this means that the use of refined beam models may be ineffective if geometrical nonlinear relations are not employed. These phenomena become particularly evident in thin-walled/shell-like type structures.*

Keywords: Carrera unified formulation; Higher-order beam models; Geometrical nonlinear relations.

---

1 Introduction

Beam theories are an important means for the study of a large number of structural problems in many engineering fields, such as mechanical, civil and aerospace. Compared to two-dimensional (2D) and three-dimensional (3D) models, one-dimensional (1D) theories provide a great advantage in terms of computational costs when dealing with slender structures. Early theories include the classical models of Eulero-Bernoulli [1], Saint-Venant [2, 3] and Timoshenko [4]. According to these models, the three-dimensional problem is reduced into a one-dimensional one, which depends only on the axial coordinate along the beam length (axis). A detailed analysis and discussion of these classical theories have been provided in many works, for example by Mucichescu [5].
Classical beam theories are based on the assumption of rigid cross-sections. Nevertheless,

*Professor of Aerospace Structures and Aeroelasticity
†Assistant Professor. Corresponding author. E-mail: alfonso.pagani@polito.it
‡Post Graduate Research Assistant. E-mail: riccardo.augello@polito.it

the analysis of more general structures, such as thin-walled beams, and the need to detect in-plane distortion, local effects and warping, may require the use of specific and refined beam theories. Many refined beam theories are available in the literature. A discussion of various models can be found, for instance, in Kapania and Raciti [6, 7], who provide a review of several beam and plate theories for vibration, buckling, and post-buckling, with particular attention to models that account for transverse shear-deformation. A comprehensive discussion about higher-order beam models for the linear analysis of metallic structures can be found in the review paper by Carrera et al. [8] and Carrera and Petrolo [9]. A comprehensive review of theories of beam-like structures is provided in the book of Hodges [10].

The local effects that may occur in the structures are more evident when they are subjected to loadings that lead to large displacements and large rotations. The nonlinear geometric relations shall be taken into account when these phenomena are current. Based on the classical Euler-Bernoulli beam theory [1], efficient solutions for this problem are represented by the works of Barten [11] and Rodhe [12], who analyzed cantilever beams undergoing concentrated and distributed loads. The problem of beams in the large deflection field was also investigated by Conway [13], regarding simply supported beams, and Wang [14], who addressed numerical analysis for these problems. Bažant and Cedolin [15] proved that it is necessary to carry out a 3D analysis to detect all the local effects and the post-buckling, that may occur within the structure. Bathe and Bolourchi [16] proposed an updated Lagrangian and a total Lagrangian formulation of a 3D beam element, showing its computational efficiency. However, in the presence of local effects or higher-order phenomena, the implementation of refined beam models in the geometrically nonlinear analysis is mandatory. Simo and Vu-Quoc [17] considered a three-dimension rod model accounting for torsional warping of its cross-section. Ibrahimbegović and Frey [18] used finite element analysis to discuss the geometrical nonlinear behavior of elastic beams, considering the shear deformation, referring to the Reissner work [19]. In the literature, works on the nonlinear analysis of thin-walled structures can be found:for example, the book from Doyle [20]. Chan and Kitipornchai [21] derived nonlinear governing equations for thin-walled elements, including second order nonlinear terms, and Kang and Yoo [22] analyzed the buckling behavior of thin-walled circular beams in the large displacement field. In this work, an higher-order formulation is used to evaluate geometrical nonlinearities due to large cross-sectional deformations and large rotations on beam structures. As qualitatively shown in Fig. 1, beams can exhibit relevant displacements over the cross-section. Figure 1(a) shows that classical beam theories are not able to catch any cross-section displacement and deformation. Figure 1(b) shows the evaluation over the cross-section using refined beam theories. The problems we address in this paper are the following: are the geometrically

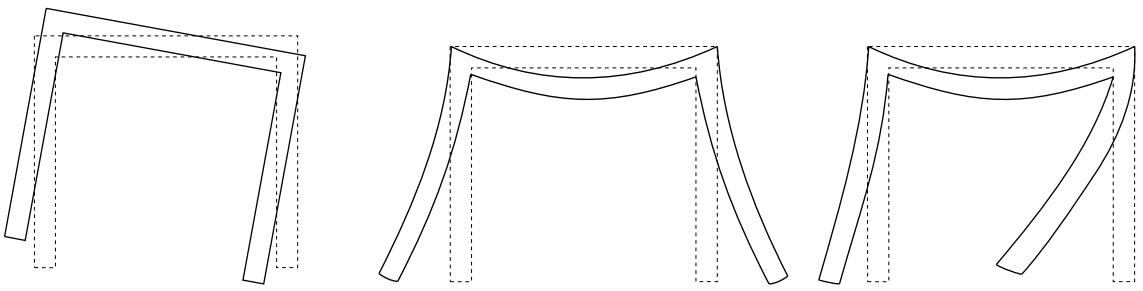

(a) Rigid rotations from classical theories

(b) Cross-section deformations by refined beam theories

Figure 1: Cross-section deformation for different beam theories

linear models able to exactly describe the cross-section deformations and rotations, which

are described by refined beam models of Fig. 1(b)? Does an higher-order (i.e., kinematically nonlinear) model require the use of nonlinear displacement-strain relations? What is the accuracy with respect to the section geometry? This work will demonstrate with practical examples that, even if higher-order theories are applied to calculate the displacement field over the cross-section, the geometrical nonlinear relations must be taken into account to be able to catch the correct displacement field, for a given class of problems. To make that more clear, consider the Green-Lagrange strain tensor. The strains along the three Cartesian axes x,y,z are:

$$\begin{aligned}
\epsilon_{xx} &= u_{x_{,x}} + \frac{1}{2}({u_{x_{,x}}}^2 + {u_{y_{,x}}}^2 + \overset{(Section)}{\boxed{{u_{z_{,x}}}^2}}) \\
\epsilon_{yy} &= u_{y_{,y}} + \frac{1}{2}({u_{x_{,y}}}^2 + {u_{y_{,y}}}^2 + \overset{(Flexure)}{\boxed{{u_{z_{,y}}}^2}}) \\
\epsilon_{zz} &= u_{z_{,z}} + \frac{1}{2}(\overset{(Section)}{\boxed{{u_{x_{,z}}}^2}} + {u_{y_{,z}}}^2 + {u_{z_{,z}}}^2)
\end{aligned} \tag{1}$$

where y is the beam axis, and x and z are the coordinates along the beam axis. (see Fig. 2), while u_x, u_y, u_z are the correspondent displacements, respectively. The term ${u_{z_{,y}}}^2$ regard the nonlinearity along the beam axis, whereas ${u_{z_{,x}}}^2$ and ${u_{x_{,z}}}^2$ are those within the cross-section. Figure 2 shows the notation used. The $u_z,_y^2$ component of the Eq. 1 would be required to describe the displacement of the beam in its global bending, while the use of $u_z,_x^2$ and $u_x,_z^2$ could be mandatory to catch the nonlinearities over the cross-section. It appears evident that to approach the problem appropriately it would be necessary to use both higher-order theory and geometrically nonlinear models. In this paper the higher-order beam model is derived in

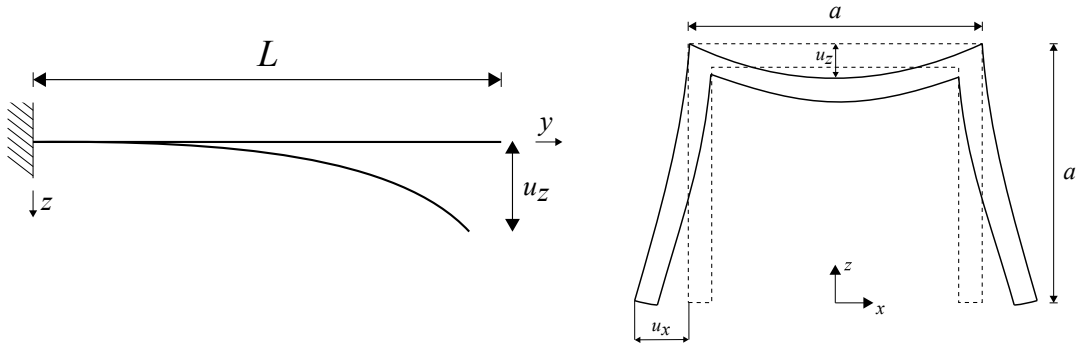

(a) Overall (b) Section

Figure 2: Main displacement components in the global bending and local cross-section deformation for a thin-walled beam.

the framework of the Carrera Unified Formulation (CUF) [23], whose extension to nonlinear problems was given in [24].

CUF is a hierarchical formulation that considers the order of the structural model as an input of the analysis so that no specific formulations are needed to obtain any refined models. Any higher-order theory is obtained by means of the so called "fundamental nuclei" (FN), which form is independent on the order of the expansion used to express the displacements unknowns on the cross-section. CUF has been applied to solve various problems, including post-buckling [24], and thin-walled cross-section [25]. Further examples of CUF applications are the hygrothermal analysis [26], micromechanics [27], thermo-elastic response [28, 29] and

free vibration analysis [30], among the others. CUF has been recently extended to nonlinear geometric problems, for both metallic and composite structure [24, 31]. This paper is organized as follows: (i) first, some preliminary and introductory information is given in Section 2, including the kinematic relations and the constitutive expressions for elastic metallic materials, and the formulation of the refined beam theory used, namely the CUF and the Finite Element Method (FEM); (ii) subsequently, Section 3 briefly describes the nonlinear governing equations and the *fundamental nuclei* of secant and tangent matrices for the solution of the geometrically nonlinear problem; (iii) then, numerical results are discussed for different loading and structural cases in Section 4; (iv) finally, the main conclusions are drawn.

2 Higher-order beam element

2.1 Constitutive and geometric relations

In this study, we consider beam elements with arbitrary cross-sections and they lay on the x-z plane of a Cartesian reference system. The y coordinate is the direction of the beam axis. Before introducing the constitutive and geometric relations, it is important to state that in this work, for convenience purpose, stress and strain tensors are expressed in vectorial form.

$$\boldsymbol{\sigma} = \left\{ \begin{array}{cccccc} \sigma_{xx} & \sigma_{yy} & \sigma_{zz} & \sigma_{xz} & \sigma_{yz} & \sigma_{xy} \end{array} \right\}^T, \quad \boldsymbol{\epsilon} = \left\{ \begin{array}{cccccc} \epsilon_{xx} & \epsilon_{yy} & \epsilon_{zz} & \epsilon_{xz} & \epsilon_{yz} & \epsilon_{xy} \end{array} \right\}^T \tag{2}$$

Regarding the constitutive relations, a linear elastic isotropic metallic is considered. The relation between $\boldsymbol{\sigma}$ and $\boldsymbol{\epsilon}$ is thus expressed by the Hooke's law, as shown in the following equation:

$$\boldsymbol{\sigma} = \mathbf{C}\boldsymbol{\epsilon} \tag{3}$$

where $\mathbf{C}$ is the material matrix. Explicit form of matrix $\mathbf{C}$ can be found in many books, see [32, 33].
For the geometrical relations, the Green-Lagrange nonlinear strain equations are taken into account.

$$\begin{aligned}
\epsilon_{xx} &= u_{x,x} + \frac{1}{2}({u_{x,x}}^2 + {u_{y,x}}^2 + {u_{z,x}}^2) \\
\epsilon_{yy} &= u_{y,y} + \frac{1}{2}({u_{x,y}}^2 + {u_{y,y}}^2 + {u_{z,y}}^2) \\
\epsilon_{zz} &= u_{z,z} + \frac{1}{2}({u_{x,z}}^2 + {u_{y,z}}^2 + {u_{z,z}}^2) \\
\epsilon_{xz} &= u_{x,z} + u_{z,x} + u_{x,x}u_{x,z} + u_{y,x}u_{y,z} + u_{z,x}u_{z,z} \\
\epsilon_{yz} &= u_{y,z} + u_{z,y} + u_{x,y}u_{x,z} + u_{y,y}u_{y,z} + u_{z,y}u_{z,z} \\
\epsilon_{xy} &= u_{x,y} + u_{y,x} + u_{x,x}u_{x,y} + u_{y,x}u_{y,y} + u_{z,x}u_{z,y}
\end{aligned} \tag{4}$$

The displacement-strain relations can be written in a compact form by introducing the linear and nonlinear differential operators $\mathbf{b}_l$ and $\mathbf{b}_{nl}$. The relation is described in the following Eq. 5.

$$\boldsymbol{\epsilon} = \boldsymbol{\epsilon}_l + \boldsymbol{\epsilon}_{nl} = (\mathbf{b}_l + \mathbf{b}_{nl})\mathbf{u} \tag{5}$$

The complete form of these two matrices can be found in [24].

2.2 Unified beam kinematics

The beam model adopted in this work for the analyses is developed in the framework of the CUF. Here, the three-dimensional displacement field $\mathbf{u}(x,y,z) = \left\{ \begin{array}{ccc} u_x & u_y & u_z \end{array} \right\}^T$ can be expressed as a generic expansion of the primary unknowns. In the case of one-dimensional theories, one has:

$$\mathbf{u}(x,y,z) = F_s(x,z)\mathbf{u}_s(y), \qquad s = 1,2,....,M \tag{6}$$

where F_s are the expansion functions of the cross-section with coordinates x and z, $\mathbf{u}_s$ is the vector of the displacements evaluated on the beam axis, M represents the order of the expansion functions, and the subscript s denotes summation. In this formulation, any kind of 1D models can be adopted by opportunely choosing the F_s. The research work proposed in this paper makes use of three different cross-section functions: L4, which implies a bi-linear interpolation on the cross-section; L9 with quadratic interpolation; L16 with cubic interpolation. For instance, the displacement field given by L16 approximation is:

$$\begin{aligned} u_x &= F_1 u_{x_1} + F_2 u_{x_2} + F_3 u_{x_3} + F_4 u_{x_4} + F_5 u_{x_5} + ... + F_{14} u_{x_{14}} + F_{15} u_{x_{15}} + F_{16} u_{x_{16}} \\ u_y &= F_1 u_{y_1} + F_2 u_{y_2} + F_3 u_{y_3} + F_4 u_{y_4} + F_5 u_{y_5} + ... + F_{14} u_{x_{14}} + F_{15} u_{x_{15}} + F_{16} u_{x_{16}} \\ u_z &= F_1 u_{z_1} + F_2 u_{z_2} + F_3 u_{z_3} + F_4 u_{z_4} + F_5 u_{z_5} + ... + F_{14} u_{x_{14}} + F_{15} u_{x_{15}} + F_{16} u_{x_{16}} \end{aligned} \tag{7}$$

where $u_{x1}, \ldots, u_{z16}$ are the displacement at the nodes of the L16, and $F_1, ..., F_{16}$ are expansion functions. Interested readers can refer to [25] for further details.

2.3 Finite element approximation

To discretize the structure along the y axis, FEM is adopted. Thus, the generalized displacement vector $\mathbf{u}_s(y)$ is approximated as expressed in the following equation:

$$\mathbf{u}_s(y) = N_j(y)\mathbf{q}_{sj} \qquad j = 1,2,\ldots,p+1 \tag{8}$$

where N_j stands for the j-th shape function, p is the order of the shape functions, j indicates summation and $\mathbf{q}_{sj}$ is the vector of the FE nodal parameters. It is important to note that the choice of the expansion functions for the cross-section, in terms of both class and size, is independent of the finite beam element used to discretize the displacement along the beam axis.

Finally, Eq. 5 can be written with the introduction of the CUF (Eq. 6) and FEM (Eq. 8) relations. In this way, the strain vector can be written in algebraic form as follows:

$$\boldsymbol{\epsilon} = (\mathbf{B}_l^{sj} + \mathbf{B}_{nl}^{sj})\mathbf{q}_{sj} \tag{9}$$

where $\mathbf{B}_l^{sj}$ and $\mathbf{B}_{nl}^{sj}$ are the linear and nonlinear algebraic matrices.

3 Nonlinear governing FE equations

Equilibrium equation is derived from stationary conditions via the principle of virtual work, which states that the virtual variation of the strain energy (δL_{int}) is equal to the virtual variation of the work of the external loads (δL_{ext}). By adopting the notation described in the

previous section and as shown in Eq. 2, the virtual variation of the internal strain energy can be written as:

$$\delta L_{\text{int}} = \int_V \delta\boldsymbol{\epsilon}^T \boldsymbol{\sigma}\, dV \tag{10}$$

Starting from Eq. 10, considering the constitutive equations for elastic materials (Eq. 3) and the geometric relation Eq. 9, one can write:

$$\delta L_{\text{int}} = \delta \mathbf{q}_{\tau i}^T \left(\int_V \left(\mathbf{B}_l^{\tau i} + 2\,\mathbf{B}_{nl}^{\tau i} \right)^T \mathbf{C} \left(\mathbf{B}_l^{sj} + \mathbf{B}_{nl}^{sj} \right) dV \right) \mathbf{q}_{sj} \tag{11}$$

Equation 11, and in particular the argument of the integral, can be written in terms of FNs. The result is the secant stiffness matrix $\mathbf{K}_S^{ij\tau s}$, that is made of the sum of the following four contributions:

$$\begin{cases} \displaystyle\int_V \mathbf{B}_l^{\tau i}\,\mathbf{C}\,\mathbf{B}_l^{sj}\, dV = \mathbf{K}_0^{ij\tau s} & \textit{linear contribution} \\ \displaystyle\int_V \mathbf{B}_l^{\tau i}\,\mathbf{C}\,\mathbf{B}_{nl}^{sj}\, dV = \mathbf{K}_{lnl}^{ij\tau s} & \textit{nonlinear contribution of order 1} \\ \displaystyle\int_V 2\,\mathbf{B}_{nl}^{\tau i}\,\mathbf{C}\,\mathbf{B}_l^{sj}\, dV = \mathbf{K}_{nll}^{ij\tau s} & \textit{nonlinear contribution of order 1} \\ \displaystyle\int_V 2\,\mathbf{B}_{nl}^{\tau i}\,\mathbf{C}\,\mathbf{B}_{nl}^{sj}\, dV = \mathbf{K}_{nlnl}^{ij\tau s} & \textit{nonlinear contribution of order 2} \end{cases} \tag{12}$$

Concerning the FN of the tangent stiffness matrix, $\mathbf{K}_T^{ij\tau s}$, it is derived from the linearization of the equilibrium equations, see [24]. We assume that the loading is conservative so that the linearization of the virtual variation of the external loads is zero. Formally, the tangent matrix can be obtained from linearizing the virtual variation of the strain energy as follows:

$$\begin{aligned} \delta(\delta L_{\text{int}}) &= \textstyle\int_V \delta(\delta\boldsymbol{\epsilon}^T\boldsymbol{\sigma})\, dV \\ &= \textstyle\int_V (\delta\boldsymbol{\epsilon}^T\delta\boldsymbol{\sigma}) + (\delta(\delta\boldsymbol{\epsilon}^T)\boldsymbol{\sigma})\, dV \end{aligned} \tag{13}$$

where the first term is calculated as follows:

$$\int_V \delta\boldsymbol{\epsilon}^T\delta\boldsymbol{\sigma} dV = \delta\mathbf{q}_{\tau i}^T \left(\int_V (\mathbf{B}_l^{\tau i} + 2\,\mathbf{B}_{nl}^{\tau i})^T \mathbf{C}\, (\mathbf{B}_l^{sj} + 2\,\mathbf{B}_{nl}^{sj}))\, dV \right) \delta\mathbf{q}_{sj} \tag{14}$$

As done for the Eq. 11, Eq. 14 can be written in terms of the FN, as shown in the following system:

$$\begin{cases} \int_V \mathbf{B}_l^{\tau i}\,\mathbf{C}\,\mathbf{B}_l^{sj}\,dV & = & \mathbf{K}_0^{ij\tau s} & \textit{linear contribution} \\ \int_V \mathbf{B}_l^{\tau i}\,\mathbf{C}\,2\,\mathbf{B}_{nl}^{sj}\,dV & = & 2\,\mathbf{K}_{lnl}^{ij\tau s} & \textit{nonlinear contribution of order 1} \\ \int_V 2\,\mathbf{B}_{nl}^{\tau i}\,\mathbf{C}\,\mathbf{B}_l^{sj}\,dV & = & \mathbf{K}_{nll}^{ij\tau s} & \textit{nonlinear contribution of order 1} \\ \int_V 2\,\mathbf{B}_{nl}^{\tau i}\,\mathbf{C}\,2\,\mathbf{B}_{nl}^{sj}\,dV & = & 2\,\mathbf{K}_{nlnl}^{ij\tau s} & \textit{nonlinear contribution of order 2} \end{cases} \tag{15}$$

Note that $\mathbf{K}_0^{ij\tau s}$, $\mathbf{K}_{lnl}^{ij\tau s}$, $\mathbf{K}_{nll}^{ij\tau s}$, and $\mathbf{K}_{nlnl}^{ij\tau s}$ are the same 3×3 FNs as given in Eq. 11.
The second term of the Eq. 13 is:

$$\int_V \delta(\delta\boldsymbol{\epsilon}^T)\boldsymbol{\sigma}\,dV \;=\; \delta\mathbf{q}_{\tau i}^T \mathbf{K}_\sigma^{ij\tau s}\delta\mathbf{q}_{sj} \tag{16}$$

where $\mathbf{K}_\sigma^{ij\tau s}$ is often called the geometric stiffness matrix. The explicit form of the FN of both secant and tangent stiffness matrix and the omitted steps for the solution of the Eq. 16 can be found in [24]. A vast numerical investigation has been made to study the effects of section deformation vs nonlinear effects. Several results are described in the following subsections. Assessment of the nonlinear model is given in previous works [24, 31]. Also, in these works, the complete procedure that is used in the present investigation for the resolution of the nonlinear equations, and which make us of a Newton-Raphson method along with a path following constraint, is described in detail.

4 Numerical results

4.1 Compact cross-section beam

To show the relationships between the kinematics of higher-order theories and the nonlinear displacement-strain relations, a square compact cross-section of a beam is considered first. The beam is made of an aluminium alloy with Young modulus E equal to 75 GPa and Poisson ratio $\nu = 0.33$, and it is subjected to clamped-free boundary conditions. The geometry of the cross-section is shown in Fig. 3, with side $w = 0.1$ m. The beam has length $L = 2$ m. Two loadings P are applied at two opposite sides of the cross-section, as depicted in the

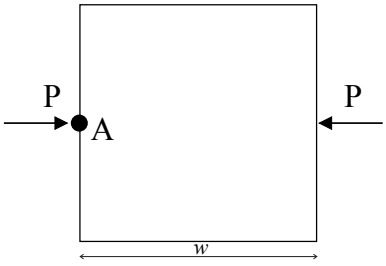

Figure 3: Cross-section geometry and loading condition for the compact square beam.

figure. To take into account higher-order theories, 1L4, 1L9 and 1L16 Lagrange polynomial

discretizations have been adopted for the description of the cross-section, as shown in Fig. 4. Increasing forces have been applied to the structure, until it reaches the tensile yield strength which, for the aluminum alloy chosen, is 503 MPa. Both linear and nonlinear analyses are

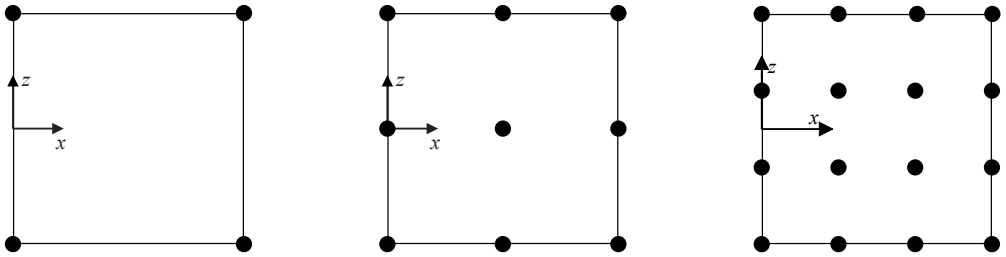

(a) (b) (c)

Figure 4: Cross-section discretization for the compact cross-section beam.

conducted, and the displacement in the x-direction of the middle point of the upper side of the cross-section (the point "A" in Fig. 3) has been evaluated. Then, the percentage difference between linear and nonlinear solutions has been plotted in Fig. 5. The results show that the greater the order of the beam theory, the higher the difference between linear and geometric nonlinear analyses. Nevertheless, the values of the percentage differences are not relevant from the engineering perspective, hence linear analyses could be considered quite accurate for the compact beam analyzed in this section. Figure 5 shows that even with a high order theory

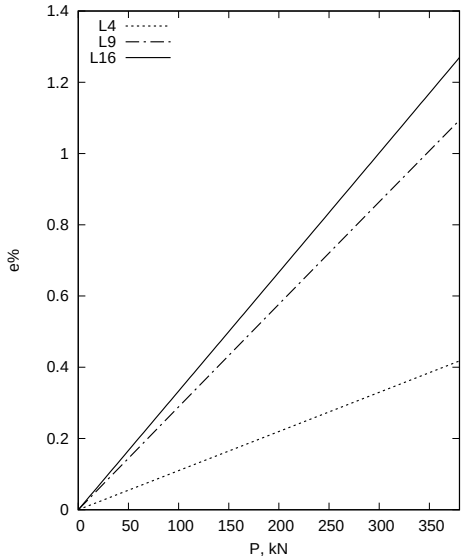

Figure 5: Percentage difference between linear and geometric nonlinear analyses for compact square cross-section beam.

for the calculation of the displacement field over the compact cross-section, the difference between linear and nonlinear solutions is low. For the sake of completeness, some significant displacement values are reported in Table 1. Main results results are highlighted in bold, showing that the difference between linear and nonlinear solutions increases from 0.4 for a linear beam theory to 1.1 for a quadratic beam theory and 1.3 to a cubic model.

	$L4$			$L9$			$L16$		
P	$-u_{xl}$	$-u_{xnl}$	$e_{\%}$	$-u_{xl}$	$-u_{xnl}$	$e_{\%}$	$-u_{xl}$	$-u_{xnl}$	$e_{\%}$
9.997	0.004	0.004	0.011	0.010	0.010	0.029	0.008	0.008	0.033
52.68	0.020	0.020	0.058	0.051	0.051	0.152	0.044	0.044	0.175
128.3	0.048	0.048	0.141	0.123	0.124	0.370	0.106	0.107	0.427
256.7	0.097	0.096	0.097	0.246	0.248	0.740	0.213	0.215	0.857
392.4	0.149	0.148	**0.431**	0.376	0.381	**1.129**	0.325	0.329	**1.311**

Table 1: Values of the displacement and error of the compact cross-section, for various beam theory orders and both linear and geometric nonlinear solutions. The load is expressed in kN, the displacements are expressed in $mm \times 10^3$.

4.2 Thin-walled beam

The second analysis deals with a thin-walled channel-section beam. The geometry is shown in Fig. 6, with $w = 0.1$ m, $h = 0.1$ m and $t = 0.01$ m. The length of the beam is $L = 2$ m. The material properties are the same as in the previous case. Three different higher-order

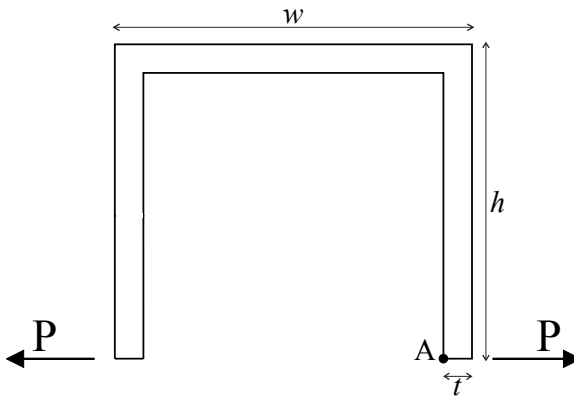

Figure 6: Cross-section geometry and loading condition for the open section beam.

models are used to describe the channel-section and to calculate the displacement field, and they differ in the order and number of Lagrange polynomials adopted on the cross-section. In detail, 8L4, 8L9 and 8L16 have been implemented, as shown in Fig. 7. Increasing forces

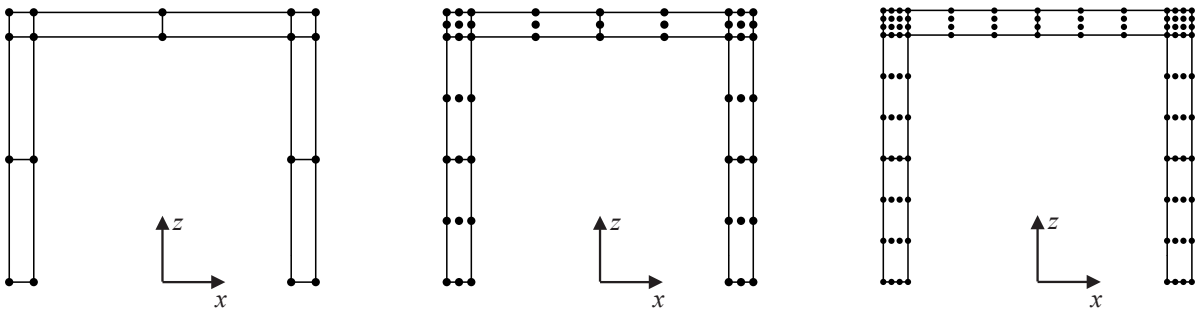

(a) 8L4 discretization (b) 8L9 discretization (c) 8L16 discretization

Figure 7: Cross-section discretization for the open section beam.

have been applied to the structure until the stress reaches the tensile yield strength. In this

scenario, linear and nonlinear analyses are conducted and the displacement of the point "A" along x-axis is evaluated. The difference between linear and nonlinear solutions is calculated and shown in Fig. 8. In this case, the percentage difference in higher-order theory including

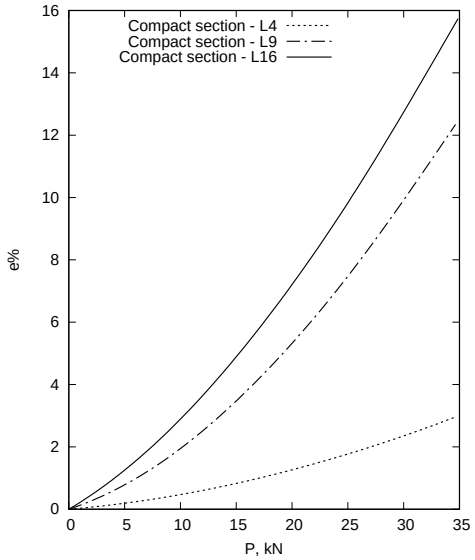

Figure 8: Percentage difference between linear and geometrical nonlinear analyses for open cross-section.

or not the nonlinear terms is more than 10 times greater than in the previous compact cross-section case (Fig. 5). The three higher-order theories present the same behavior as in the previous case. By increasing the external loading, the percentage difference increases. This trend can be better appreciated in Table 2, where some values of both linear and nonlinear solution are reported. High difference percentages between linear and nonlinear analyses are

	$L4$			$L9$			$L16$		
P	$-u_{xl}$	$-u_{xnl}$	$e_{\%}$	$-u_{xl}$	$-u_{xnl}$	$e_{\%}$	$-u_{xl}$	$-u_{xnl}$	$e_{\%}$
1.503	0.498	0.498	0.049	1.314	1.311	0.193	1.363	1.358	0.335
6.377	2.099	2.094	0.258	5.571	5.512	1.064	5.776	5.681	1.665
16.94	5.564	5.626	1.017	14.80	14.21	4.157	15.31	14.49	5.735
25.62	8.338	8.508	1.888	22.38	20.77	7.764	23.13	21.00	10.12
35.08	11.29	11.64	**3.044**	30.63	27.21	**12.57**	31.60	27.30	**15.74**

Table 2: Values of the displacement and error of the compact cross-section beam, for various beam theory orders and for both linear and geometric nonlinear solutions. The load is expressed in kN, the displacements are expressed in $mm \times 10^3$.

quoted in bold in the table. These values goes from 3.0 for a first order beam model to 12.6 for a quadratic beam model and to 15.7 to a cubic theory. It is clear that for these thin-walled problems the use of higher-order theory requires the use of nonlinear geometrical relations.

4.3 Thin-walled pinched cylinder

As a final example, a thin-walled pinched cylinder has been analyzed. Material and geometrical data have been taken from a very well known shell problem problem by Flügge [34]. The

material has Young modulus $E = 3 \times 10^6$ psi and Poisson ratio $\nu = 0.3$. The geometry is shown in Fig. 9, with length $L = 600$ in, radius $r = 300$ in and thickness $t = 3$ in. As in

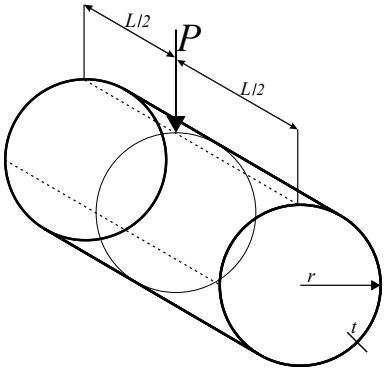

Figure 9: Cross-section geometry and loading condition for the pinched cylinder.

the previous cases, three different higher-order beam models have been utilized to evaluate the displacement field over the cross-section. For completeness reasons, Table 3 shows the comparison of solutions from the present beam model and the one provided by Flügge. As

Model	*Displacement*
Flügge	0.15118
*L*4	0.08479
*L*9	0.15107
*L*16	0.15174

Table 3: Values of the displacement of the point B in the linear solution, compared to that from Flügge [34]. The load is equal to $1lb$, the displacement are expressed in $in \times 10^{-4}$.

shown in Fig. 10, 30 Lagrange polynomials are spaced over the cross-section and they are progressively smaller, in order to ensure more accurate results in the position of the applied load (the decrease of the polynomials is linear so that $A_1/A_2 = 10$). Both static linear and

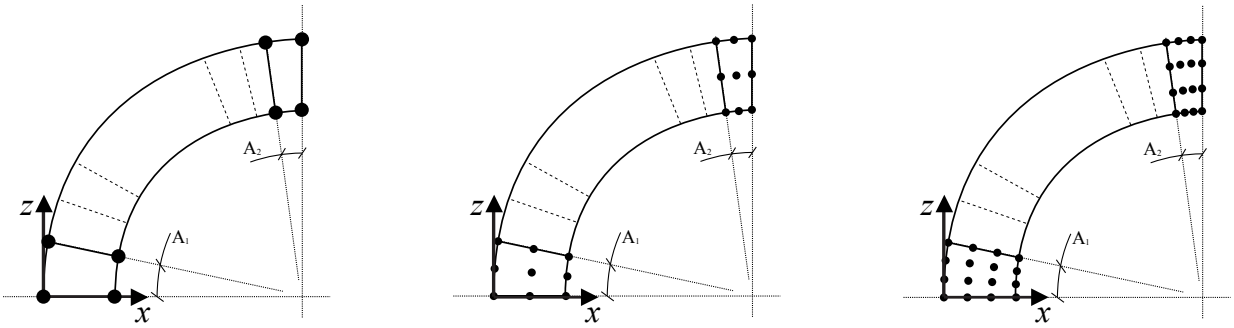

(a) 30L4 discretization (b) 30L9 discretization (c) 30L16 discretization

Figure 10: Cross-section discretization for the pinched cylinder.

nonlinear analysis have been performed and the percentage difference between the linear and nonlinear solution has been evaluated. In Fig. 11, the z component of the displacement of the point B (in the cross-section depicted in the figure) was taken into account and the results show how L9 and L16 polynomials lead to the almost same results, while the L4 solution

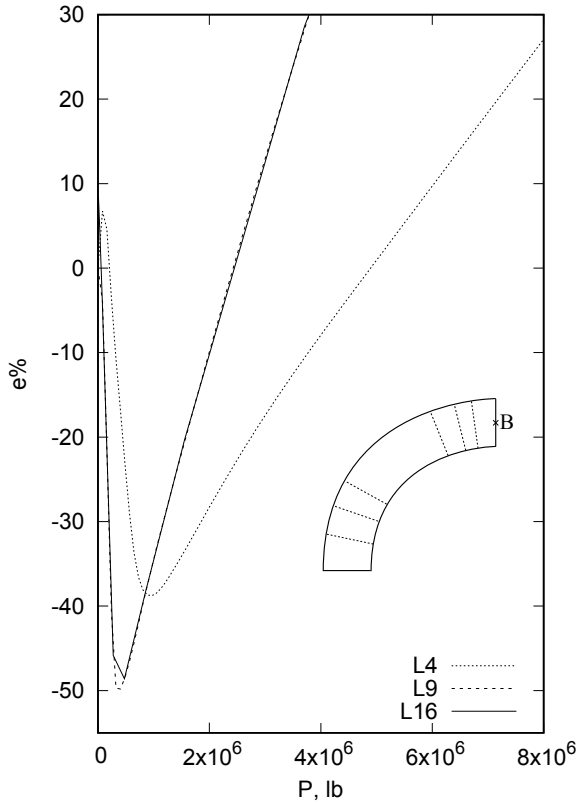

Figure 11: Percentage difference between linear and nonlinear analyses results for the pinched cylinder.

is completely different. Moreover, for all the dicretization, the error is null for some given positions on the cross-section. The reason is that, before this value, the displacement from the nonlinear solution is higher than the linear solution one, as can be seen in Fig. 12(a), while it becomes less increasing the external load, as shown in Fig. 12(b) (in Fig. 12 the differences between linear and nonlinear solutions can be better appreciated. Some of the most important displacement and error values are reported in Table 4. To better appreciate the

	$L4$			$L9$			$L16$		
P	$-u_{zl_b}$	$-u_{znl_b}$	$e_{\%}$	$-u_{zl_b}$	$-u_{znl_b}$	$e_{\%}$	$-u_{zl_b}$	$-u_{znl_b}$	$e_{\%}$
10.10	0.080	0.085	0.737	0.141	0.153	8.434	0.141	0.153	8.460
80.20	0.634	0.678	5.855	1.276	1.212	−4.052	1.268	1.217	−3.998
272.6	2.512	2.312	−5.943	7.591	4.119	−45.17	7.368	4.137	−45.83
3707	35.09	31.43	−10.67	43.54	56.00	28.05	43.74	56.25	28.60
10928	60.67	91.64	**51.06**	64.16	165.1	**152.2**	65.00	165.8	**155.2**

Table 4: Values of the displacement and error of the thin-walled cylinder, for various beam theory orders and for both linear and geometric nonlinear solutions. The load is expressed in $lb \times 10^3$, the displacements are expressed in in.

difference from the three theories, another displacement has been evaluated: in Fig. 13(a), in fact, point C has been taken into account, leading to evident differences between the L16 solution and the other two. Moreover, in 13(b) the percentage error of the values of the von Mises stress in point C are evaluated, showing the same trend as the other figure for the pinched cylinder.

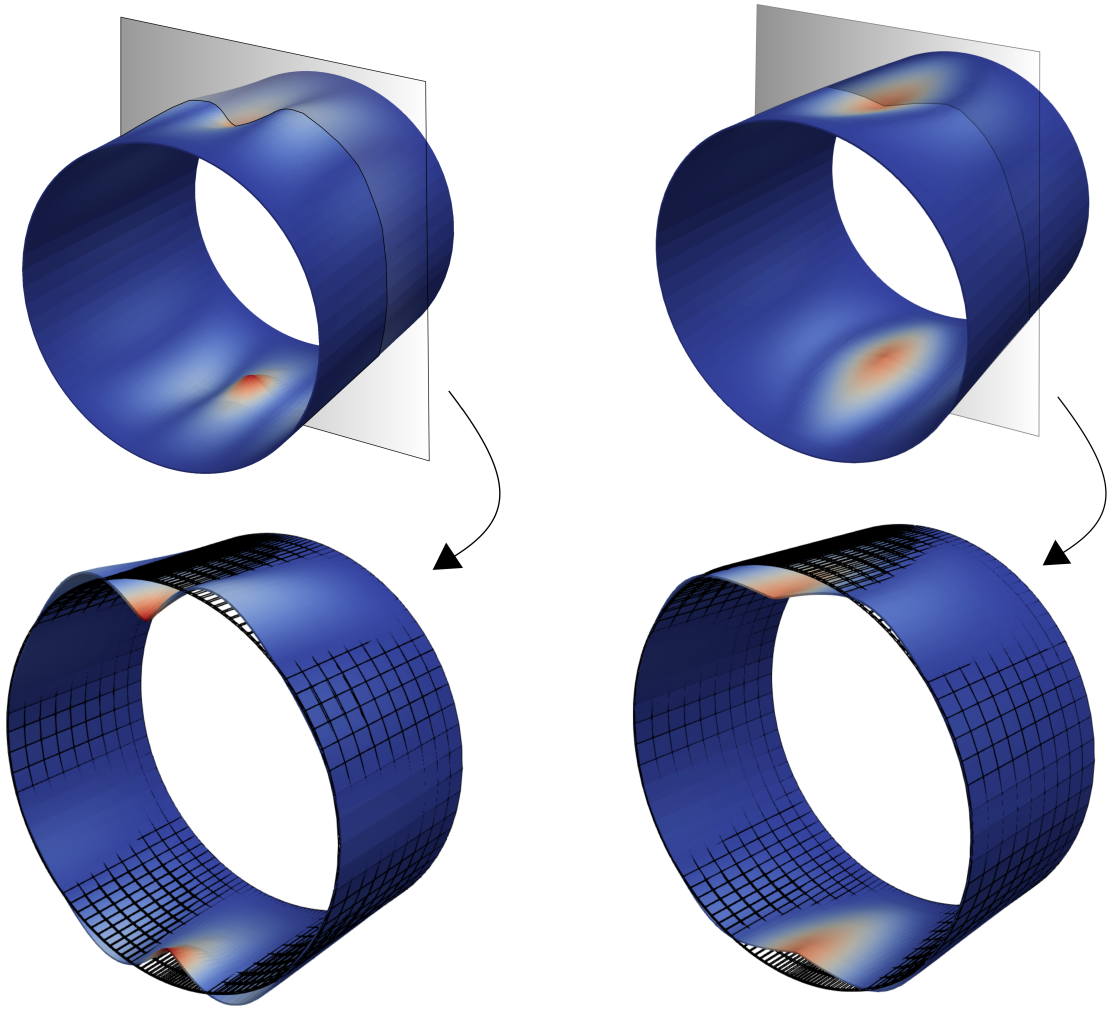

(a) *Linear solution* (b) *Nonlinear solution*

Figure 12: Global deformation shapes of the thin-walled cross-section beam for the L16 polynomials configuration.

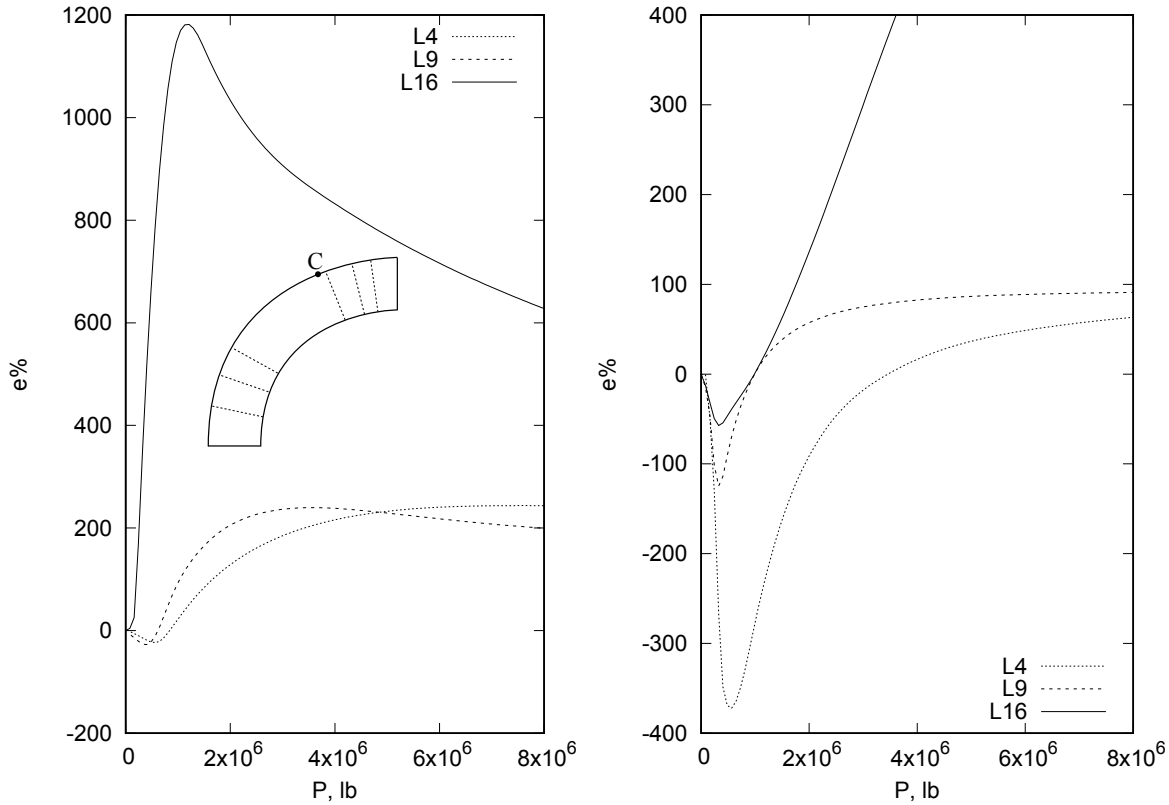

Figure 13: Percentage difference about the displacement and von Mises stress value at the point C, between linear and nonlinear analyses.

5 Conclusions

The effectiveness of geometrical nonlinear relations in higher-order models of beams and shell-like structures has been investigated in this work. By employing the Carrera Unified Formulation (CUF), different higher-order theories have been addressed in the domain of linear and nonlinear elasticity. Different cross-sections have been analyzed, and in particular, it has been shown that the geometrical nonlinear kinematic relations can be very significant on thin-walled type structures. It has been proved that in many problems the use of refined beam model must be accomplished by a geometrical nonlinear formulation to correctly capture the deformed state of the given structure.

References

[1] L. Euler. *Methodus Inveniendi Lineas Curvas Maximi Minimive Proprietate Gaudentes Sive Solutio Problematis Isoperimetrici Latissimo Sensu Accepti*, volume 1. Springer Science and Business Media, 1952.

[2] A. de Saint-Venant. *Mémoire sur la Flexion des Prismes*. Gauthier-Villars, 1856.

[3] A. de Saint-Venant. *Mémoire sur la Flexion des Prismes*. Imprimerie nationale, 1856.

[4] S. P. Timoshenko. On the transverse vibrations of bars of uniform cross-section. *The London, Edinburgh, and Dublin Philosophical Magazine and Journal of Science*, 43(253):125–131, 1922.

[5] D. T. Mucichescu. Bounds for stiffness of prismatic beams. *Journal of Structural Engineering*, 110(6):1410–1414, 1984.

[6] R. K. Kapania and S. Raciti. Recent advances in analysis of laminated beams and plates. Part I: Sheareffects and buckling. *AIAA journal*, 27(7):923–935, 1989.

[7] R. K. Kapania and S. Raciti. Recent advances in analysis of laminated beams and plates. Part II: Vibrations and wave propagation. *AIAA journal*, 27(7):935–946, 1989.

[8] E. Carrera, A. Pagani, M. Petrolo, and E. Zappino. Recent developments on refined theories for beams with applications. *Mechanical Engineering Reviews*, 2(2):14–00298, 2015.

[9] E. Carrera and M. Petrolo. On the effectiveness of higher-order terms in refined beam theories. *Journal of Applied Mechanics*, 78(2):021013, 2011.

[10] D. H. Hodges. Nonlinear composite beam theory. *Progress in Astronautics and Aeronautics*, 213:304, 2006.

[11] H. J. Barten. On the deflection of a cantilever beam. *Quarterly of Applied Mathematics*, 2(2):168–171, 1944.

[12] F. Rohde. Large deflections of a cantilever beam with uniformly distributed load. *Quarterly of Applied Mathematics*, 11(3):337–338, 1953.

[13] H. D. Conway. Xciv. the large deflection of simply supported beams. *The London, Edinburgh, and Dublin Philosophical Magazine and Journal of Science*, 38(287):905–911, 1947.

[14] T. M. Wang. Non-linear bending of beams with uniformly distributed loads. *International Journal of Non-Linear Mechanics*, 4(4):389–395, 1969.

[15] Z. P. BazÏant and L. Cedolin. *Stability of structures: elastic, inelastic, fracture and damage theories*. World Scientific, 2010.

[16] K.-J. Bathe and S. Bolourchi. Large displacement analysis of three-dimensional beam structures. *International Journal for Numerical Methods in Engineering*, 14(7):961–986, 1979.

[17] J. C. Simo and L. Vu-Quoc. A geometrically-exact rod model incorporating shear and torsion-warping deformation. *International Journal of Solids and Structures*, 27(3):371–393, 1991.

[18] A. Ibrahimbegović and F. Frey. Finite element analysis of linear and non-linear planar deformations of elastic initially curved beams. *International journal for numerical methods in engineering*, 36(19):3239–3258, 1993.

[19] E. Reissner. On one-dimensional finite-strain beam theory: the plane problem. *Zeitschrift für angewandte Mathematik und Physik ZAMP*, 23(5):795–804, 1972.

[20] J. F. Doyle. *Nonlinear Analysis of Thin-Walled Structures: Statics, Dynamics, and Stability*. Springer Science & Business Media, 2013.

[21] S. L Chan and S. Kitipornchai. Geometric nonlinear analysis of asymmetric thin-walled beam-columns. *Engineering Structures*, 9(4):243–254, 1987.

[22] Y. J. Kang and C. H. Yoo. Thin-walled curved beams. i: formulation of nonlinear equations. *Journal of Engineering Mechanics*, 120(10):2072–2101, 1994.

[23] E. Carrera, G. Giunta, and M. Petrolo. *Beam Structures: Classical and Advanced Theories*. John Wiley & Sons, 2011.

[24] A. Pagani and E. Carrera. Unified formulation of geometrically nonlinear refined beam theories. *Mechanics of Advanced Materials and Structures*, 25(1):15–31, 2018.

[25] E. Carrera and M. Petrolo. Refined beam elements with only displacement variables and plate/shell capabilities. *Meccanica*, 47(3):537–556, 2012.

[26] M. Cinefra, M. Petrolo, G. Li, and E. Carrera. Hygrothermal analysis of multilayered composite plates by variable kinematic finite elements. *Journal of Thermal Stresses*, 40(12):1502–1522, 2017.

[27] I. Kaleel, M. Petrolo, A. M. Waas, and E. Carrera. Computationally efficient, high-fidelity micromechanics framework using refined 1d models. *Composite Structures*, 181:358–367, 2017.

[28] A. Entezari, M. Filippi, and E. Carrera. Unified finite element approach for generalized coupled thermoelastic analysis of 3d beam-type structures, part 1: Equations and formulation. *Journal of Thermal Stresses*, 40(11):1386–1401, 2017.

[29] M. Filippi, A. Entezari, and E. Carrera. Unified finite element approach for generalized coupled thermoelastic analysis of 3d beam-type structures, part 2: Numerical evaluations. *Journal of Thermal Stresses*, 40(11):1402–1416, 2017.

[30] E. Carrera, M. Petrolo, and P. Nali. Unified formulation applied to free vibrations finite element analysis of beams with arbitrary section. *Shock and Vibration*, 18(3):485–502, 2011.

[31] A. Pagani and E. Carrera. Large-deflection and post-buckling analyses of laminated composite beams by carrera unified formulation. *Composite Structures*, 170:40–52, 2017.

[32] K. J. Bathe. *Finite Element Procedure*. Prentice hall, Upper Saddle River, New Jersey, USA, 1996.

[33] T. J.R. Hughes. *The Finite Element Method: Linear Static and Dynamic Finite Element Analysis*. Courier Corporation, 2012.

[34] W. Flügge. *Stresses in Shells*. Springer, Berlin, 2nd edition, 1960.